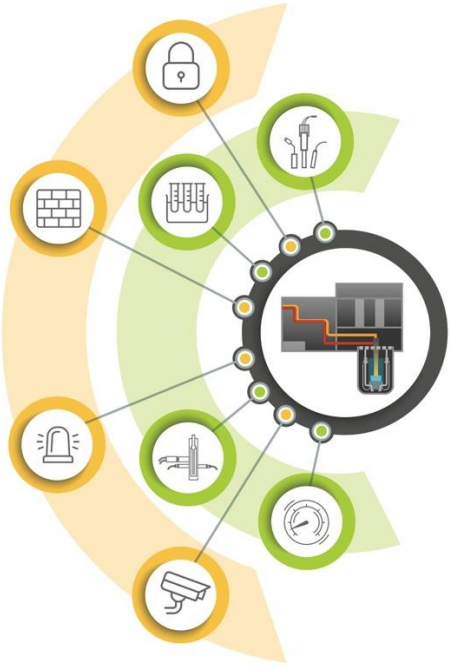

On-line Monitoring for Molten Salt Reactor MC&A: Optical Spectroscopy-Based Approaches

Prepared for
US Department of Energy

A.M. Lines, S.A. Bryan,
H.M. Felmy, and S.D. Branch

Pacific Northwest National Laboratory

September 2022
PNNL-33367

SUMMARY

Molten salt reactors (MSRs) represent a key green energy technology that can meet changing world energy demands. Within the United States, support and interest for these reactor designs can be observed, including examples of DOE support through the Advanced Reactor Demonstration Program (ARDP) and GAIN. Significant technological progress is being made with MSR reactor design, but questions still remain in how material control and accounting (MC&A) approaches can be translated or created for MSR processes.

The ability to spectroscopically measure oxidation states of uranium was demonstrated for U(III), U(IV) and U(IV) within various chloride eutectics. These were performed by the sequential addition of U(III) and U(IV) in the chemical forms of UCl_3 and UCl_4, respectively into a dual UV-vis/Raman spectroscopic cell while measuring the spectroscopic signatures of the solution species. The UV-vis and Raman spectroscopic methods followed the chemical conversion of U(III) to U(IV) and U(IV) to U(VI) during the heating periods of these experiments. The quantitative conversion of each species transition was confirmed by on-line monitoring and principal component regression modeling of the solution phase. The molar absorptivities for U(IV) and U(VI) were confirmed to be consistent with literature for the UV-vis and Raman spectra of these species. The U(III) molar absorptivity calculated in this work was smaller than the reported value, but with the knowledge that U(III) oxidizes under the salt conditions studied here and real melt concentrations are lower than those calculated based on mass addition, a lower molar absorptivity would be expected. In addition, the limits of detection for U(III), U(IV), and U(VI) were determined for these techniques.

Salts characterized included salts provided by an industrial partner, TerraPower. These salts were representative of anticipated industry conditions and included salts of clean chloride eutectics, UCl_3, and fission products simulants. Data from these systems was included in the chemometric modeling to both build and challenge models in the quantification of U in various oxidation states and in melts that contained complex matrices/interferents. Overall, work indicates optical spectroscopy can be successfully implemented to follow U species within salt melts. Uncertainties of current models are higher than those achieved via traditional offline analysis, but continuous monitoring may offer significant MC&A benefits within deployed reactors. It should be emphasized that given budgets, instrumentation utilized here included general spectrometers already existing in the laboratory. While results generally indicated low limits of detection and uncertainty, these results could be further improved by procuring instruments optimized to provide higher resolution and sensitivity at the spectral points of interest to U. Furthermore, extended data sets including higher concentrations of U or access to more developed loops with advanced control of U oxidation state could further reduce uncertainties. Either of these advancements could be pursued in future work. These details along with modeling results and future opportunities will be discussed within this report.

Details included here walk through the analysis of U in increasingly complex salt melts. Examples first focus on the optical fingerprints of U in simplistic systems, e.g., U in salts that have been cleaned and without any other interfering analytes present. Note, because of the tendency of U to disproportionate, these melts are automatically complicated by the presence of multiple oxidation states of U. Discussion then covers how those U fingerprints can be impacted within salt matrices that may not be clean (i.e. moisture or hydroxides are present) and as well as how the presence of fission products and fission product simulants can interfere with U signals. This data is then used to build chemometric models for quantification of U in all three available oxidation states of U (III, IV, and VI), where models are built and compared between simple (U only) and complex (U in the presence of fission product simulants) salt melts. Resulting model metrics then demonstrate how accuracy is impacted by the presence of interfering species. This is used to calculate uncertainty of measurement which is discussed in the context of meeting MC&A requirements and needs.

CONTENTS

SUMMARY iii

ACRONYMS AND ABBREVIATIONS ix

1. INTRODUCTION 1

2. SETUP AND METHODOLOGIES 3
   2.1. Small-Scale Molten Salt Setup 3
   2.2. Inert Box Setup 3
   2.3. Salt Conditions 4

3. RESULTS AND DISCUSSION 4
   3.1. Overview of Uranium Fingerprints 5
   3.2. Overview of Interferent Fingerprints 8
   3.3. Chemometric modeling 14
      3.3.1. Initial models on simplistic systems 15
      3.3.2. Advancing models to include interfering species 16
      3.3.3. Application of chemometric models on full spectral datasets containing mixtures of U(III), U(IV), and U(VI) 17

4. UNCERTAINTIES, BENEFITS AND MC&A APPLICATIONS 20

5. CONCLUSIONS 22

6. ACKNOWLEDGEMENTS 23

7. REFERENCES 24

FIGURES

Figure 1-1. Roadmap for on-line monitoring technology development[14]. 2

Figure 2-1. Schematic of the small-scale furnace system showing the cuvette inside a clam-shell furnace with both Raman and UV-vis optics connected via fiber optics to the spectroscopic instruments. 3

Figure 2-2. Photos of A) commercially available and subsequently cleaned LiK-Cl eutectic melted in a quartz cuvette at 550°C and B) NaMg-Cl eutectic acquired from TerraPower melted at 500°C. 4

Figure 3-1. Optical fingerprint of U(III) in NaMg-Cl collected at 700 °C showing the conversion over time of U(III) to U(VI) in A) a 3D plot over time, B) a 2D plot showing the decrease in U(III) signature and increase in U(VI) signature, and C) a calibration curve and LOD. 6

Figure 3-2. Optical fingerprint U(IV) in NaKMg-Cl at 550 °C showing A) 3D plot of the spectra of each addition of U(IV) into blank NaKMg-Cl eutectic, B) averaged spectra of each addition of U(IV), and C) calibration curve and calculated LOD based on the average intensity of the U(IV) band at 670 nm versus added U(IV) concentration. 7

Figure 3-3. Optical fingerprint U(VI) in NaKMg-Cl at 550 °C showing A) UV-vis spectra showing conversion of U(IV) to U(VI), B) calibration curve and calculated LOD from the intensity of the U(VI) band at 455 nm versus the concentration of U(VI), D) Raman spectra showing the increasing concentration of U(VI), and D) calibration curve and calculated LOD from the intensity of the U(VI) band at 842 cm^{-1} versus concentration of U(VI). 7

Figure 3-4. Interfering signal from fission products: A) 3D plot of spectra measured while adding $NdCl_3$ and $ErCl_3$, B) averaged spectra measured after each addition of Nd^{3+} or Er^{3+}, C) photo of the sapphire tube used containing a Nd^{3+} salt and D) a Nd^{3+} and Er^{3+} mixture. These measurements were done in a LiK-Cl eutectic salt at 500 °C. 9

Figure 3-5. A) Spectra of variable U(IV) and U(VI) in NaKMg-Cl molten salt; B) spectra of various lanthanides in molten chloride salt matrix; and C) combined U(IV)/U(VI) spectra with spectra of various lanthanides syntactically added. 10

Figure 3-6. A) Photo of blank NaMg-Cl salt melted at 550 °C and B) Photo of the salt after the addition of a U(III) with mixed fission products. 11

Figure 3-7. A) Raman spectra collected at 550 °C after the addition of a U(III) sample mixed with fission products, B) Raman spectra of a Nd^{3+} melt and a Nd^{3+} with Er^{3+} salt melt measured during the experiment described in Figure 3-4, and C) UV-vis spectrum of U(III) after the addition of a U(III) sample containing mixed fission products. 11

Figure 3-8. UV-vis spectra of melted blank salts: LiK-Cl, cleaned LiK-Cl, NaKMg-Cl, and TerraPower NaMg-Cl eutectic salts referenced to an empty quartz cuvette and ranging in temperature from 500 – 700 °C. 13

Figure 3-9. A) Optical fingerprint of U(IV) and U(III) in cleaned LiK-Cl, B) averaged spectra after each addition of U(IV) or U(III), C) absorbance of primary U(IV) and U(III) peaks after each of the 6 additions of either U(IV) or U(III). Demonstrates ability to account for target species in “impure” salt. 14

Figure 3-10. Parity plots for the principal component regression modeling of U(III), U(IV), and U(VI) based on UV-vis spectra in NaKMg-Cl eutectic solution. 15

Figure 3-11. Parity plot for the principal component regression (PCR) modeling of U(VI) Raman spectra in NaKMg-Cl eutectic solution. 16

Figure 3-12. The direct measurement of U(IV) and U(VI) in a NaKMg-Cl eutectic. U(IV) was added (as UCl_4 salt) in six sequential steps (U(IV)-1 through U(IV)-6, black dashed line), while U(IV) (green curve), U(VI) (yellow curve), and their sum (magenta curve) were directly and quantitatively measured via chemometric regression models. 18

Figure 3-13. Validation set for U(III)/U(IV)/U(VI) in LiK-Cl salt eutectic. Indicates ability to account for U species originally added to matrix, and ability to account for complex chemistry within matrix. 19

TABLES

Table 3-1 Weight % and molar concentration LODs along with molar absorptivities (ε) for the major U(III), U(IV), and U(VI) peaks measured using UV-vis and Raman spectroscopy. 8

Table 3-2. Comparison of relevant molar absorptivities for actinides and lanthanides in molten salt media. 12

Table 3-3. Metrics for model performance of U(III), U(IV), and U(VI). 17

ACRONYMS AND ABBREVIATIONS

ARDP	Advanced Reactor Demonstration Program
DOE	US Department of Energy
FY	fiscal year
GAIN	Gateway for Accelerated Innovation in Nuclear
LOD	limit of detection
LWR	light water reactor
MC&A	material control and accounting
MSR	molten salt reactor
PC	principal component
PCR	principal component regression
PNNL	Pacific Northwest National Laboratory
RMSEC	root mean square error of calibration
RMSECV	root mean square error of cross-validation
UV-vis	ultra-violet visible spectroscopy

1. INTRODUCTION

Molten salt reactors (MSRs) represent a key opportunity to efficiently meet growing green energy needs. As one of the key advanced reactor designs within the United States, designs proposed by various vendors have received media attention and financial support from DOE and through ARDP and GAIN awards. Numerous technological advancements and demonstrations/deployments are currently being completed. Focusing on the liquid fuel reactors, it is important to note that designs represent a major change in how radioactive inventory is spread through a facility. This can be further complicated by designs that include some form of on-line refueling, processing, or salt clean up. Overall, traditional material control and accounting (MC&A) approaches used for light water reactors (LWRs) may be difficult to translate to MSR systems.

Overall, on-line monitoring may offer a key opportunity to follow these more complex molten salt systems. This not only enables highly representative *in situ* characterization but can provide the unique benefit of continuous monitoring as compared to the discreet and infrequent MC&A completed via grab sample analysis. Furthermore, careful monitoring of system design may also offer a method to catch precipitation or precursors to precipitation that may otherwise impact accurate MC&A. The challenge here is developing or converting monitoring technology that can be applied to molten salt systems. The high temperatures (~500 °C) and corrosive environments challenge many current system designs.

Fortunately, several technologies can provide highly useful MC&A information and can be adapted to the molten salt environment. A technology of interest here is optical spectroscopy, which can provide unparalleled insight into chemical speciation, redox states, and concentrations.[1-7] This information can be highly valuable in accurately accounting for actinides that display complex chemistry under molten salt conditions. Furthermore, optical monitoring approaches can be combined with advanced analysis techniques such as chemometric modeling for the real-time and accurate analysis of optical data.[8-13] However, transitioning these technologies to molten salt systems requires key technology advances, which were identified and outlined in a previous report,[14] with Figure 1-1 below outlining the key areas. This roadmap summarizes advancements needed to produce a viable tool for MC&A of U,[5] Pu,[15-17] and Np[18]within molten salt systems.

Project work in fiscal year (FY) 2022 was focused on determining the feasibility of optical spectroscopy as a tool for MC&A of U species within a molten salt. Work focused on building optical training sets of U within multiple oxidation states across a range of concentrations. Furthermore, capabilities to identify and quantify U within highly complex melts were explored. It is anticipated that various fission products and corrosion products will have optical fingerprints that interfere with signals of target species (here U as a demonstration species). To capture this, experiments included the addition of lanthanides to explore interferences and challenge chemometric models for U quantification.

Of particular interest is the inclusion of industry representative salts provided by TerraPower. These included clean chloride eutectics, UCl_3, and fission product simulants. Data from these samples was included both in chemometric model building and validation to determine applicability to the complex salts under conditions anticipated in real MSR deployments.

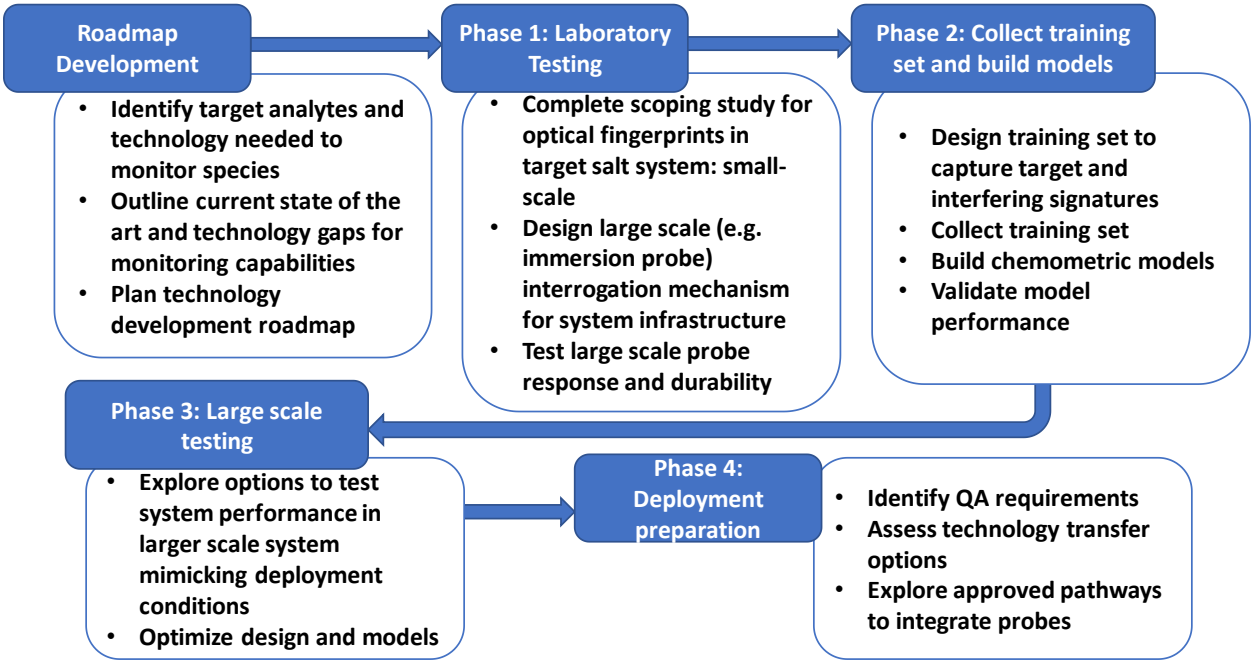

Figure 1-1. Roadmap for on-line monitoring technology development.[14]

2. SETUP AND METHODOLOGIES

Molten salt characterization poses an experimental challenge due to the high temperatures, corrosive nature of the salts, and the need for an inert atmosphere. The sections below detail the experimental parameters used to conduct optical spectroscopic measurements of molten salts to enable the characterization and quantification of U in multiple oxidation states and in the presence of interfering species.

2.1. Small-Scale Molten Salt Setup

A small-scale furnace system was utilized for this work. The system was preexisting and described in more detail elsewhere.[1-3] Figure 2-1 below shows a schematic of the furnace system which is capable of holding a quartz cuvette or other optically transparent sample holder. Both Raman and UV-vis spectroscopy can be measured simultaneously to monitor U in different oxidation states and in the presence of interfering species.

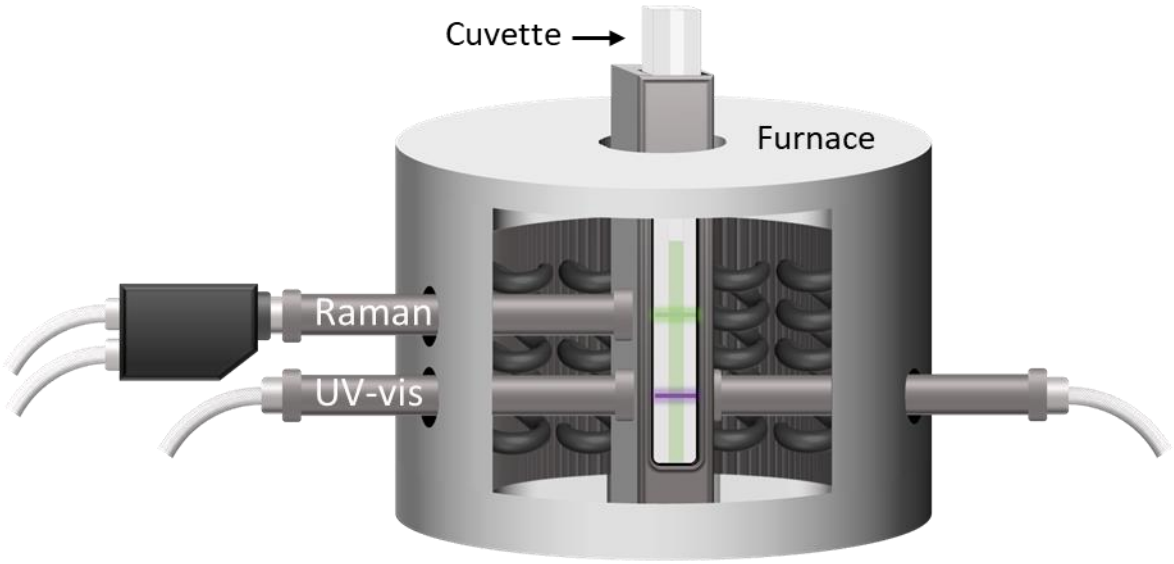

Figure 2-1. Schematic of the small-scale furnace system showing the cuvette inside a clam-shell furnace with both Raman and UV-vis optics connected via fiber optics to the spectroscopic instruments.

Raman and UV-vis spectroscopic instruments were acquired from Spectra Solutions Inc. and each utilize thermoelectrically-cooled charge-coupled device detectors. The UV-vis instrument had a functional wavelength range of approximately 450 – 850 nm. The Raman instrument used was either a system with a 532 nm (340 mW) diode laser, a spectral range of approximately 100 – 4000 cm^{-1}, and a resolution of ~3 cm^{-1} or a system with a 220 mW 532 nm diode laser with approximately 400 – 4200 cm^{-1} spectral range and ~2 cm^{-1} resolution. All instruments utilized SpectraSoft software for data collection.

2.2. Inert Box Setup

An important factor in these measurements is the ability to operate the small-scale furnace system under inert atmosphere due to the hydroscopic nature of the salts used. Therefore, all of these measurements were conducted in an inert Ar atmosphere glovebox. The atmosphere in the glovebox is maintained at <0.4 ppm O_2 and <8 ppm H_2O and the box pressure is maintained at 1.7 – 2 mbar. This setup allows for the entire furnace system to be contained inside the glovebox with feedthroughs allowing connection to spectroscopic instruments and temperature controllers outside the glovebox. Cuvettes and sapphire tubes for sample

containment as well as alumina tubes used for puck additions of U were thoroughly cleaned and heated in an oven at >150 °C prior to entering the glovebox.

2.3. Salt Conditions

The chloride salts used in these measurements were either commercially available LiK-Cl or NaKMg-Cl (≥99 – 99.999% purity) or NaMg-Cl salt acquired from TerraPower. The NaKMg-Cl and NaMg-Cl were used without further purification. A cleaning process was tested on the LiK-Cl eutectic which involved successive heating steps under dynamic pumping and sparging with HCl to remove moisture and impurities. The cleaning process is described in detail elsewhere.[19] Despite procuring these salts at the highest purities available, there are still impurities present. A demonstration of this is shown in Figure 2-2 where photos of the cleaned commercially available LiK-Cl salt are compared to the NaKMg-Cl salt from TerraPower. The LiK-Cl salt appears slightly yellow while the TerraPower salt is much more transparent. This indicates a higher purity for the TerraPower salt resulting in a more optically transparent solvent better suited for spectroscopic interrogation.

The uranium (IV) chloride (99.99% Bio-Analytical Industries, Inc., Doyline, LA) was used without further purification. Uranium (III) chloride was acquired from TerraPower and used without further purification. A 33 mol% U(III) sample containing a proprietary blend of fission products was also acquired from TerraPower. Lanthanide (III) chloride salts were procured from Sigma-Aldrich at 99.9 – 99.99% purity and used without further purification.

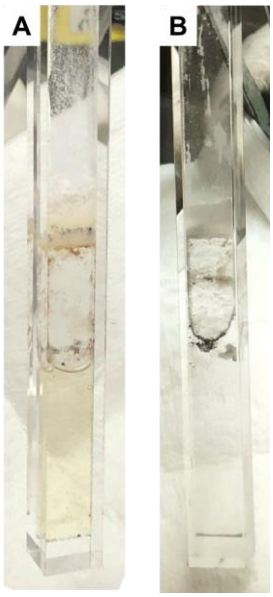

Figure 2-2. Photos of A) commercially available and subsequently cleaned LiK-Cl eutectic melted in a quartz cuvette at 550 °C and B) NaMg-Cl eutectic acquired from TerraPower melted at 500 °C.

3. RESULTS AND DISCUSSION

The primary goal of FY22 work is to determine if optical spectroscopy is a viable tool for the MC&A of molten salt systems. Previous work has already demonstrated that the optical techniques of UV-vis and Raman can be used to uniquely identify various actinides in the salt environment. These techniques can provide needed information on oxidation state and speciation, which can provide insight into behavior and

potential issues (e.g. precipitation) that could impact accurate accounting of material. This report seeks to determine the ability of these techniques to quantify targets and whether measurement uncertainties can meet MC&A requirements particularly in the presence of interfering analytes.

Data presented here includes an overview of uranium fingerprints (section 3.1), discussion of how interfering analytes impact U fingerprints (section 3.2), and a discussion on building chemometric models for quantification of U (section 3.3). Metrics such as uncertainty of measurement are discussed in section 3.3. Note, the final subsections include details on building chemometric models for the automated quantification of U within salt melts. This includes building models with simple (U only) and complex (U in the presence of fission product simulants) data sets to compare accuracy of quantification when interfering fingerprints are present. These uncertainties are provided here but are discussed in greater detail in the following section which also highlights how these fit into MC&A needs for MSRs.

3.1. Overview of Uranium Fingerprints

Uranium can assume multiple oxidation states and speciation forms within a given salt melt. Nominally, U in the 3+, 4+, and 6+ states is possible while speciation will depend on the background salt matrix and presence of interacting species. For the demonstration purposes of this work, data set collection focused on chloride salts. Several salt eutectics were explored to gain an understanding of the U fingerprint, though a wider range of focus was placed on the NaMg-Cl eutectic. Samples of this eutectic were provided by TerraPower and offered a unique opportunity to characterize a system of direct industry interest. Below is a comprehensive list of the U fingerprints characterized.

This section will focus on outlining U fingerprints in salts without interfering analytes present. This meets two goals: first this provides an overview of the U fingerprints for the reader, enabling an understanding of the complexity of signal originating from U alone, second this lays the foundation for chemometric data sets that, when combined with U in the presence of interferents, can produce robust models for quantifying U.

Figure 3-1 shows the optical response of the U(III) in molten NaMg-Cl. In this experiment, 0.27 wt% U(III) in the form of UCl_3 was added to molten NaMg-Cl at 700 °C. Upon addition of the U(III), the unique absorbance signature of the U(III) was detected, with a peak at ~570 nm and a shoulder at ~450 nm. An intense deep red color was observed, the melt was seen to be extremely turbid, and the spectroscopic signal was out of scale. As the U(III) settled to the bottom of the melt and began to dissolve into the melt, the unique U(III) spectroscopic signature diminished over the course of about 1.5 hours. This was then followed by the ingrowth of the unique signature for the uranyl U(VI) species, with a single shoulder at ~450 nm. It is likely that the U(III) rapidly oxidized to U(IV) before slowly oxidizing further to U(VI) but U(IV) signatures were not apparent, likely due to the low molar absorptivity of U(IV) and therefore low signal. Due to the extremely turbid nature of the melt upon initial addition of U(III) and the rapid rate of conversion of the U(III) species, an accurate molar absorptivity was difficult to determine. Using the known starting concentration of U(III) added and the associated absorbance, a molar absorptivity of 415 $M^{-1}cm^{-1}$ was calculated. This value is smaller than the previously reported value of 963 $M^{-1}cm^{-1}$,[20] which suggests that much of the U(III) had already oxidized before an accurate absorbance could be measured. Despite this fast oxidation, a linear calibration curve was developed. The previously reported molar absorptivity of 963 $M^{-1}cm^{-1}$ was used to calculate the concentration of U(III) remaining at the point where the first absorbance value was measured. This starting concentration and the final point where the U(III) was fully oxidized and no U(III) signature was visible, were used as the concentration values in the calibration curve. The limit of detection (LOD) was calculated using the following equation[21] where *s* is the noise from the

blank measurement and *m* is the slope of the calibration curve. The calculated LOD is reported in Table **3-1**.

$$\mathrm{LOD} = \frac{3s}{m}$$

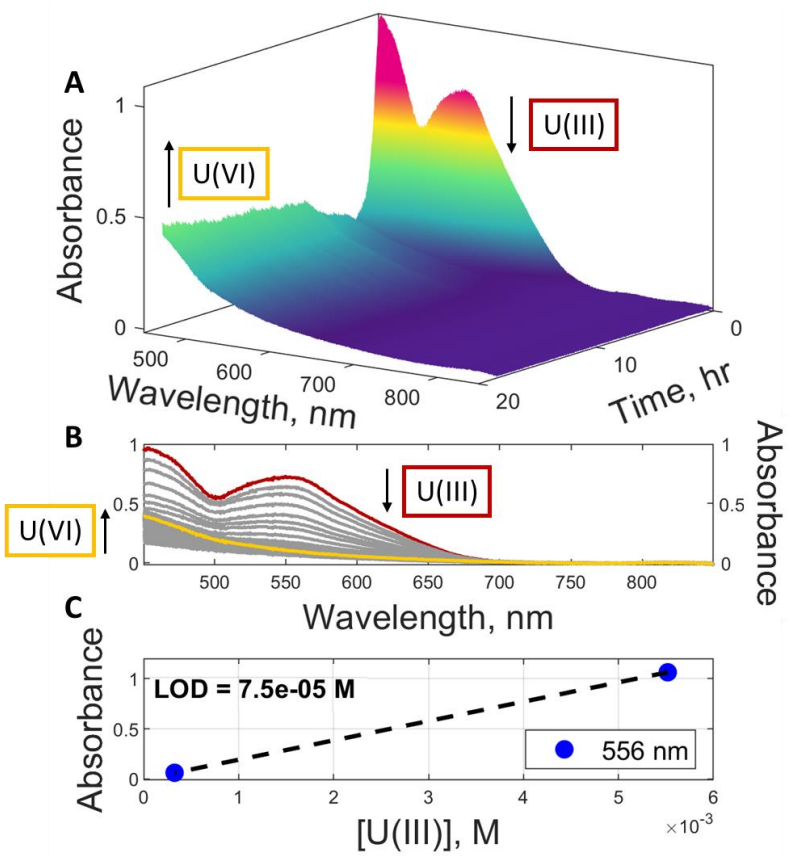

Figure 3-1. Optical fingerprint of U(III) in NaMg-Cl collected at 700 °C showing the conversion over time of U(III) to U(VI) in A) a 3D plot over time, B) a 2D plot showing the decrease in U(III) signature and increase in U(VI) signature, and C) a calibration curve and LOD.

Optical fingerprints for U(IV) and U(VI) were also measured in the molten chloride system. Figure 3-2 shows the UV-vis fingerprint for U(IV) with successive additions of UCl_4 to a molten NaKMg-Cl eutectic. This system was then allowed to equilibrate overnight (Figure 3-3) and the U(IV) was found to slowly convert to U(VI), evident by both an ingrowth of the U(VI) UV-vis band at 455 nm and an increase in the Raman signature for UO_2^{2+} at 842 cm^{-1}. Calibration curves were developed for U(IV) by UV-vis and U(VI) by both UV-vis and Raman; the calculated LODs and molar absorptivities are reported in Table 3-1. The molar absorptivities agreed with previous studies where the molar absorptivity of U(IV) determined here

was 3.5 $M^{-1}cm^{-1}$ compared to 6.47 $M^{-1}cm^{-1}$ reported previously[20] and U(VI) determined here was 60.2 $M^{-1}cm^{-1}$ compared to 57.2 $M^{-1}cm^{-1}$ reported previously[22].

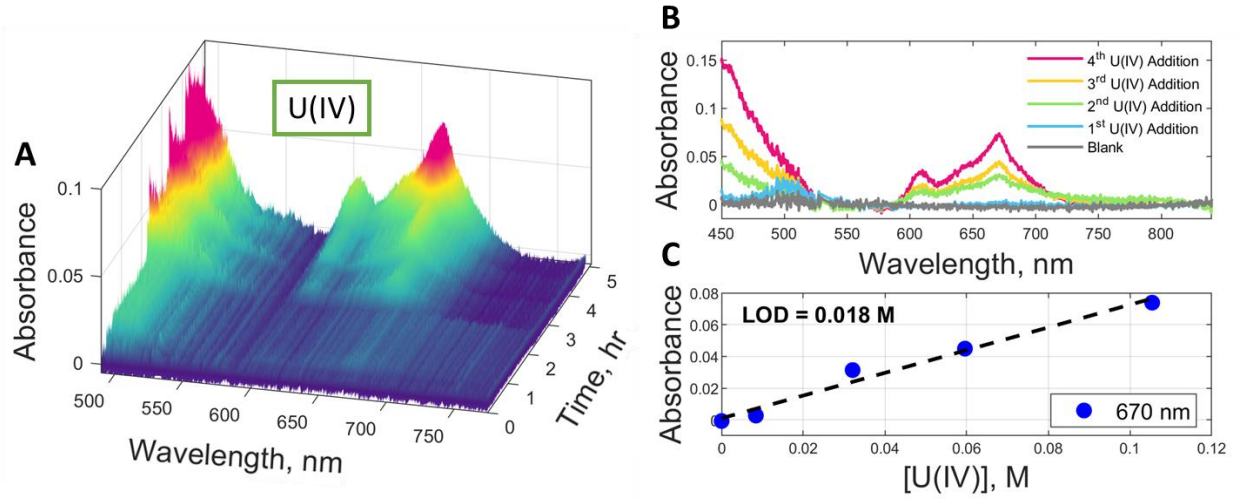

Figure 3-2. Optical fingerprint of U(IV) in NaKMg-Cl at 550 °C showing A) 3D plot of the spectra of each addition of U(IV) into blank NaKMg-Cl eutectic, B) averaged spectra of each addition of U(IV), and C) calibration curve and calculated LOD based on the average intensity of the U(IV) band at 670 nm versus added U(IV) concentration.

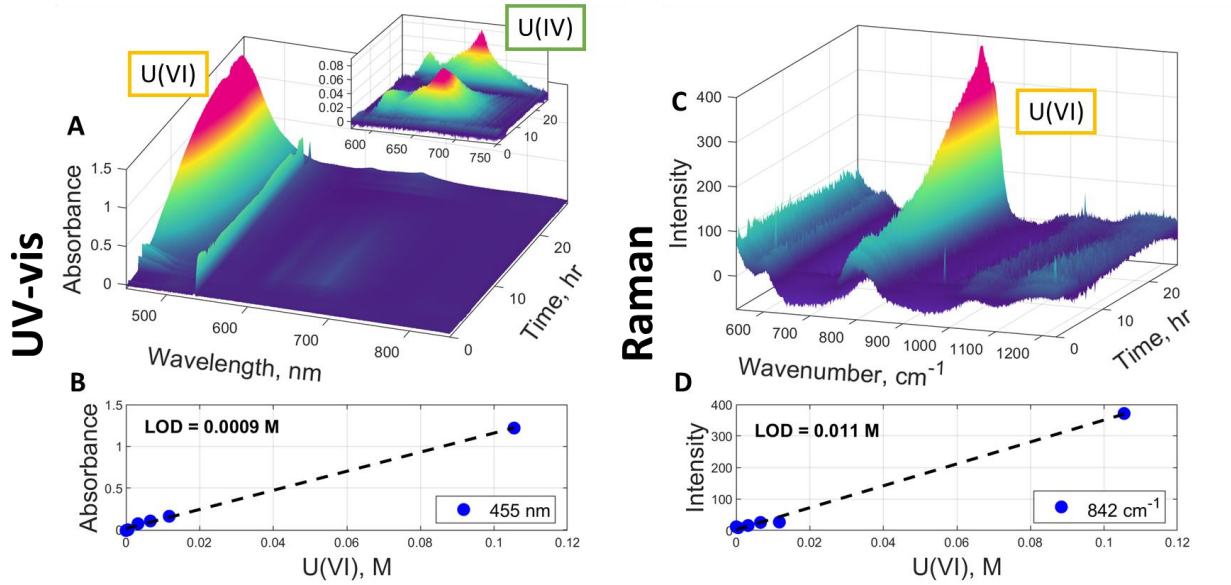

Figure 3-3. Optical fingerprint of U(VI) in NaKMg-Cl at 550 °C showing A) UV-vis spectra showing conversion of U(IV) to U(VI), B) calibration curve and calculated LOD from the intensity of the U(VI) band at 455 nm versus the concentration of U(VI), D) Raman spectra showing the increasing concentration of U(VI), and D) calibration curve and calculated LOD from the intensity of the U(VI) band at 842 cm^{-1} versus concentration of U(VI).

Table 3-1 Weight % and molar concentration LODs along with molar absorptivities (ε) for the major U(III), U(IV), and U(VI) peaks measured using UV-vis and Raman spectroscopy.

Species	Method	Peak location	LOD, wt%	LOD, M	ε, $M^{-1}\cdot cm^{-1}$
U(III)	UV-vis	556 nm	0.0016	0.000075	963*
U(IV)	UV-vis	670 nm	0.27	0.018	3.5
U(VI)	UV-vis	455 nm	0.013	0.0009	60.2
U(VI)	Raman	842 cm^{-1}	0.17	0.012	N/A

* Literature value used due to fast oxidation of U(III)[20]

These data provide a comprehensive overview of the U fingerprints within clean and industrially representative salts. The following sections will provide examples of optical impacts anticipated from salts that have not been cleaned (e.g. moisture or hydroxide impurities are present) as well as the fingerprints of fission product simulants that can interfere with measurement of U. A key item to note is the general shape of the U fingerprints. They tend to be broad (in the case of U(III)) or contain multiple peaks across the spectra range (in the case of U(IV)). This character ensures that additional fission products will interfere notably with U fingerprints, and therefore present a realistic challenge to the chemometric models.

3.2. Overview of Interferent Fingerprints

Operating molten salt systems will be highly complex, exhibiting multiple interferents that can impact or interfere with target actinide fingerprints. In on-line monitoring applications, mitigation strategies to deal with these challenges should be built into quantification algorithms. Significant prior work has outlined methods to accurately quantify targets under similar conditions or examples of data complexity.[8-9, 12] In planning towards building this capability for molten salt systems, it is important to note that interferents can fit into two primary categories:

1) Spectral fingerprint overlaps or interferes with target fingerprint(s)

2) Solution interferent chemically interacts with target species and changes target speciation and fingerprint(s)

Impacts from both these scenarios will be discussed here where the following subsections will discuss how these impacts affect accuracy and uncertainties of quantification.

Interferents with optical fingerprint overlap

Fingerprint overlap is a highly common occurrence and can typically be addressed in data analysis. Particularly, tools such as chemometric analysis can enable accurate isolation of target signals from overlapping fingerprints. This has been previously demonstrated for complex salt melts containing only lanthanides,[1] as well as on non-molten salt media exhibiting complex optical interferences.[10-12, 23-24]

Within salt melts, various fission and corrosion products are anticipated to be present and can interfere with U fingerprints. To explore impacts, this work looked at several fission product simulants. Examples of species can be seen in Figure 3-4, which shows how the ingrowth of species such as neodymium and erbium produce bands in the UV-vis optical range.

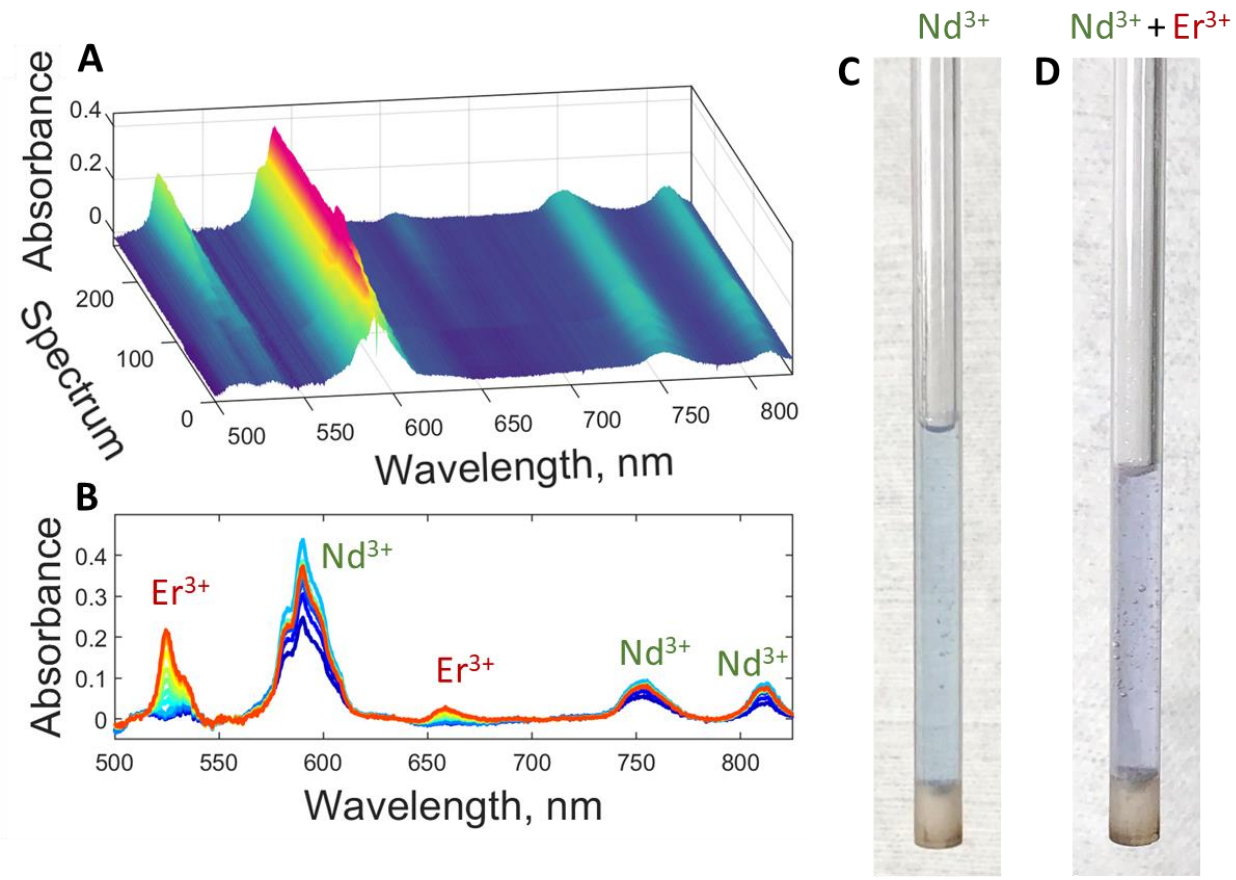

Figure 3-4. Interfering signal from fission products: A) 3D plot of spectra measured while adding $NdCl_3$ and $ErCl_3$, B) averaged spectra measured after each addition of Nd^{3+} or Er^{3+}, C) photo of the sapphire tube used containing a Nd^{3+} salt and D) a Nd^{3+} and Er^{3+} mixture. These measurements were done in a LiK-Cl eutectic salt at 500 °C.

Of greater interest is how this data will look in melts that contain the fission products in addition to the U. To first explore this, the dataset containing variable U(IV) and U(VI) modified to synthetically add in UV-vis spectra of lanthanides of known concentration measured in a separate experiment.[25] This synthetic data set allowed for a powerful initial look at how the presence of five lanthanides interfered with the signals of two oxidation states of U simultaneously present in the melt. Figure 3-5 shows the method of co-adding the U and lanthanide spectra to generate the synthetic absorbance spectra, where the original U(IV)/U(VI) spectra are shown in Figure 3-5A, with variable pure component spectra of lanthanides in Figure 3-5B. The resulting spectra shown in Figure 3-5C were constructed by adding a spectrum of each lanthanides shown in Figure 3-5B to each of the mixtures of U(IV)/U(VI) spectra in Figure 3-5A to yield the spectra shown in Figure 3-5C. The concentrations of each lanthanide selected for inclusion are: Er (100 mM), Ho (120 mM), Nd (113 mM), Pr (225 mM), Sm (252 mM), and Tm (130 mM). These resultant spectra were included in the modeling discussed in the following section.

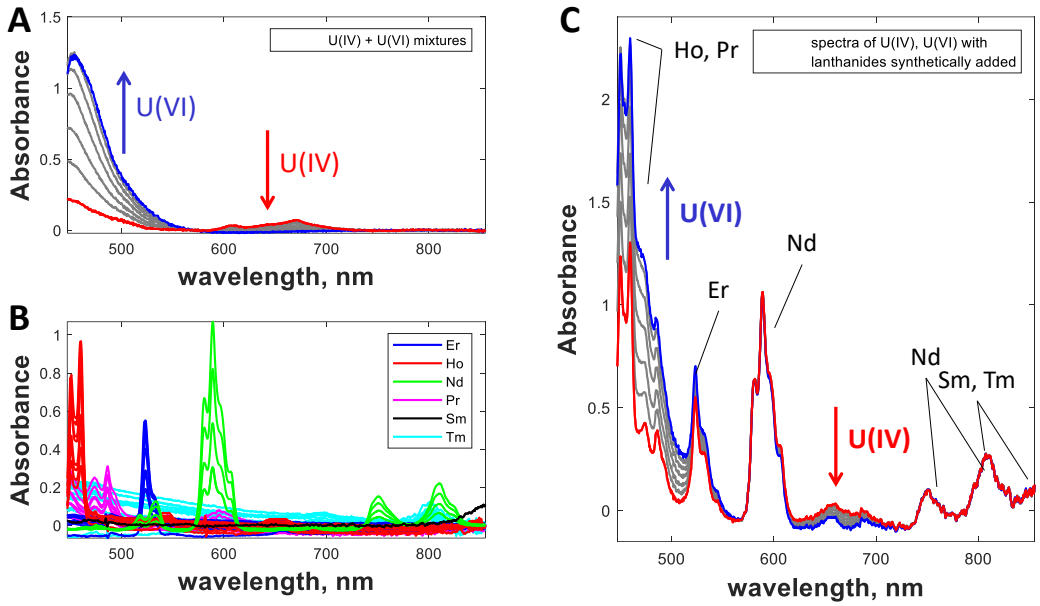

Figure 3-5. A) Spectra of variable U(IV) and U(VI) in NaKMg-Cl molten salt; B) spectra of various lanthanides in molten chloride salt matrix; and C) combined U(IV)/U(VI) spectra with spectra of various lanthanides syntactically added.

TerraPower provided an additional sample containing 33 mol% U(III) with a proprietary blend of mixed fission products in a NaMg-Cl salt which provided the opportunity to study U(III) in the presence of fission product interferants. Figure 3-6 shows photos of a melted NaMg-Cl blank salt and a photo after an addition of the U(III) mixed fission product sample. A red color is visible, consistent with U(III). There were also suspended solids which over time settled out on the bottom of the cuvette. These suspended solids caused a baseline increase in the UV-vis as light was blocked from the turbid solution. This can be seen in Figure **3-7**C where the U(III) UV-vis signature can still be seen over the baseline. Evidence of the presence of lanthanides can be seen in Figure 3-7A where broad fluorescence bands in the Raman spectrum increased after the addition of the mixed fission product sample. This was compared to Raman data collected in the Nd^{3+} and Er^{3+} samples (Figure 3-7B) described in Figure 3-4. Similar broad fluorescence bands are seen in the Nd^{3+} sample indicating that the mixed U(III) and fission product sample contained Nd. Other spectral signatures in Figure 3-7A also suggest the presence of additional lanthanides.

These results show how combining techniques can significantly improve results. In this case, the U(III) has a stronger UV-vis signal than the interfering lanthanides and Raman can measure the strong fluorescence of the lanthanides without interference from U(III), which is Raman inactive. Table 3-2 below, includes the molar absorptivities (an indication of signal strength in UV-vis) for some of the key fission products of concern as well as the target U species. This table also compares U extinction coefficients from literature and calculations here for the U species: U(III), U(IV), and U(VI). The much larger molar absorptivity of U(III) compared to Nd^{3+} (962 vs 10.7 $M^{-1}cm^{-1}$ respectively), shows why the U(III) UV-vis signal in Figure 3-7C is visible but not the Nd^{3+} bands.

Figure 3-6. A) Photo of blank NaMg-Cl salt melted at 550 °C and B) Photo of the salt after the addition of a U(III) with mixed fission products.

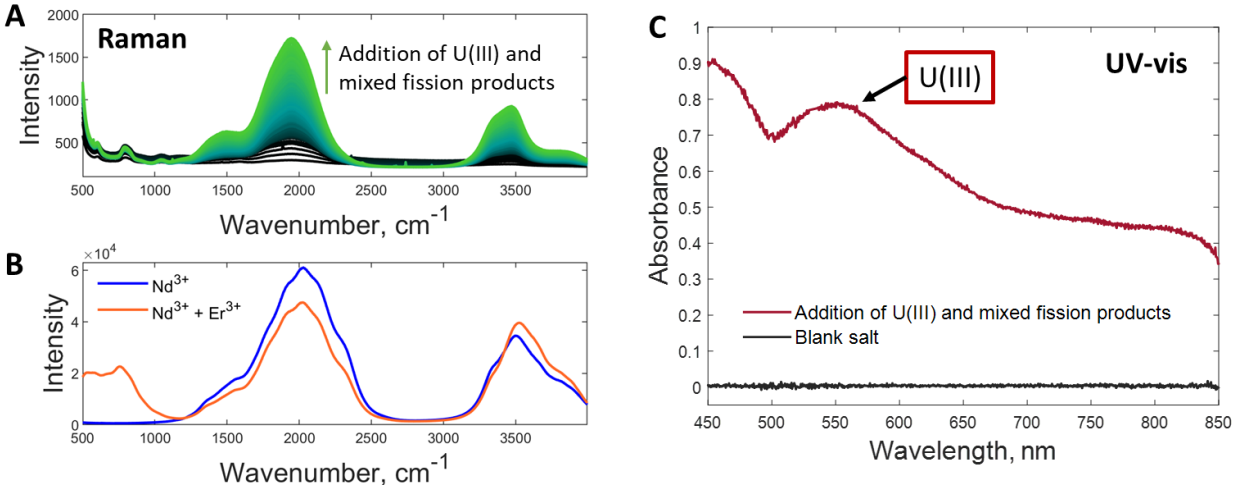

Figure 3-7. A) Raman spectra collected at 550 °C after the addition of a U(III) sample mixed with fission products, B) Raman spectra of a Nd^{3+} melt and a Nd^{3+} with Er^{3+} salt melt measured during the experiment described in Figure 3-4, and C) UV-vis spectrum of U(III) after the addition of a U(III) sample containing mixed fission products.

Table 3-2. Comparison of relevant molar absorptivities for actinides and lanthanides in molten salt media.

Species	Molar absorptivities	Reference
U(III)	A) 415 $M^{-1}cm^{-1}$ (U^{3+}, 556 nm) B) 963 $M^{-1}cm^{-1}$ (U^{3+}, 570 nm)	A) This work B) Negai, et al. (2005)
U(IV)	A) 3.5 $M^{-1}cm^{-1}$ (U^{4+}, 670 nm) B) 6.47 $M^{-1}cm^{-1}$ (U^{4+}, 670 nm)	A) This work B) Negai, et al. (2005)
U(VI)	A) 60.2 $M^{-1}cm^{-1}$ (U^{6+}, 455 nm) B) 57.2 $M^{-1}cm^{-1}$ (U^{6+}, 450 nm)	A) This work B) Negai, et al. (2004)
Nd	10.7 $M^{-1}cm^{-1}$ (Nd^{3+}, 480 nm)	Schroll, et al. (2016)
Pr	1.2 $M^{-1}cm^{-1}$ (Pr^{3+}, 486 nm)	Schroll, et al. (2016)
Pu	20 (units unclear from publication) (Pu^{3+}, 563 nm)	Bamberger, et al. (1971)
Sm	1.6 $M^{-1}cm^{-1}$ (Sm^{3+}, 408 nm)	Schroll, et al. (2016)
Eu	851 $M^{-1}cm^{-1}$ (Eu^{2+}, 330 nm) 420 $M^{-1}cm^{-1}$ (Eu^{3+}, 330 nm)	Schroll, et al. (2013)
Np	1000 $M^{-1}cm^{-1}$ (Np^{3+}, 383 nm)	Kim, et al. (2016)
Am	391 $M^{-1}cm^{-1}$ (Am^{3+}, 505 nm)	Stephanou et al. (1953)

Chemical interactions impacting target speciation and fingerprint

A more significant challenge than band overlap is the interaction of chemical species in solution that change overall fingerprints. An aqueous system corollary would be the interaction between U(VI) and Np(V) to form the new cation-cation species.[8] These new species have different fingerprints, and if not properly accounted for, can introduce significant uncertainty into materials accountancy measurements. Previous demonstrations in aqueous systems indicated accurate models can be built in the face of changing speciation.[23, 26] However, the success of these models was predicated on building training sets that captured the unique fingerprints of the different species. This can be challenging to accomplish if the chemistry or the speciation of the chemical system is not well understood. Within molten salt systems, limited literature makes this difficult. Some chemical targets, such as U, do have a good foundation in literature but most studies are completed in very pure salt systems with active chemical redox control, leaving open questions on behavior in more complex melts. It is important to note that understanding this chemistry is important for accurate material accounting regardless of approach. Optical techniques are uniquely suited to providing this type of analysis and could be an ideal avenue for future efforts of building this analysis. For the purposes of this report, this was explored in the context of building a better training set for quantifying U. Several interferents and their impacts on U behavior and fingerprints are discussed below.

Significant variability was observed in the optical transparency of the salts used in this work. As seen in Figure 3-8, the absorbance of blank chloride eutectics varied from near 0 to almost 0.5. These spectra were referenced to an empty cuvette and any measured absorbance indicates optical impurities in the salt. Overall, the NaMg-Cl salts from TerraPower gave the lowest absorbance and therefore the best optical transparency. This is not unexpected as the salts from TerraPower were run through rigorous purification processes unlike the commercially procured 99.999% pure and anhydrous salts used here. While in UV-vis measurements, blank salt spectra such as those in Figure 3-8 can be used for reference correction, starting the measurement with a high background signal limits the usable signal range and can have negative impacts on experimental results.

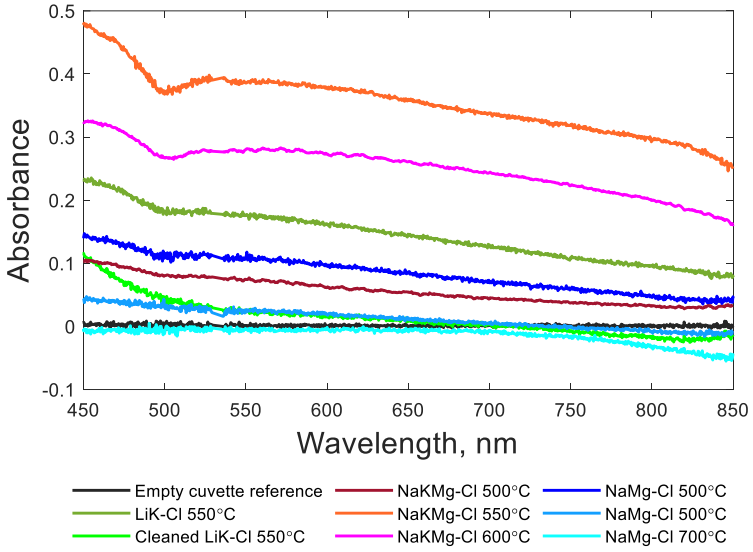

Figure 3-8. UV-vis spectra of melted blank salts: LiK-Cl, cleaned LiK-Cl, NaKMg-Cl, and TerraPower NaMg-Cl eutectic salts referenced to an empty quartz cuvette and ranging in temperature from 500 – 700 °C.

Figure **3**-9 shows the optical response of both U(III) and U(IV) in a single salt. The U(IV), in the form of UCl_4 is added incrementally to a LiK-Cl eutectic that has been purified via sparging to remove contaminants such as moisture and oxygen (Figure **3**-9A). The unique spectroscopic signatures for U(IV) (455 nm and 670 nm) begin to show and grow at a linear rate with the increase in U(IV) concentration (Figure 3-9C). Figure **3**-9B shows a 2D view of the spectra after each addition of U(IV) and U(III). Upon the addition of the U(III) species, in the form of UCl_3, the unique spectroscopic signatures for U(III) (480 nm and 563 nm) also increase. The proportional ingrowth of the U(III) species is impacted by the presence of the U(IV) species already in the melt (Figure **3**-9C). What is important to note is that despite the uranium being in what is considered an "impure" salt, optical spectroscopy can still be used to accurately measure target species, and therefore detect changes to the chemical environment of a complex salt.

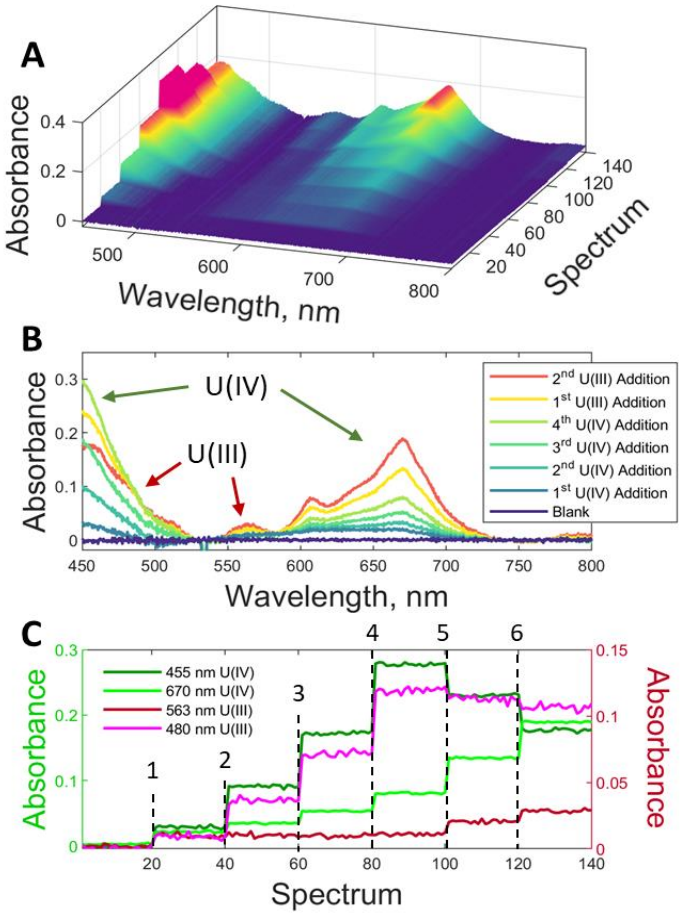

Figure 3-**9**. A) Optical fingerprint of U(IV) and U(III) in cleaned LiK-Cl at 550 °C, B) averaged spectra after each addition of U(IV) or U(III), C) absorbance of primary U(IV) and U(III) peaks after each of the 6 additions of either U(IV) or U(III).

3.3. Chemometric modeling

As demonstrated in the previous sections, the optical techniques of Raman and more specifically UV-vis absorbance can uniquely capture the signals of U in multiple oxidation states.[9, 27] This is demonstrated both on single component (e.g. single oxidation states of U), and multicomponent (e.g. multiple oxidation states of U both with and without other interfering analytes present) salt melts. The previous sections also provide some initial insight into how optical techniques can be used to quantify targets, including the presentation of single variate calibration curves and calculated limits of detection. However, complex salts (see section 3.2 for examples) make the application of single variate analysis highly challenging and results in large uncertainties.

Fortunately, through the use of chemometric modeling – a multivariate analysis approach – highly accurate quantification of U can be achieved.[9, 27] This section details how collected data sets are used to build models, and, more importantly, provides an overview of quantification accuracy and uncertainty. This is completed for single and multicomponent salt systems.

3.3.1. Initial models on simplistic systems

Separate UV-vis and Raman models were generated to follow the various U(III), U(IV), and U(VI) species in solution. Results in this section focus on providing insight into model performance when single component (or nearly so) U data sets are used to build models.

Using the UV-vis spectral data from Figure 3-1, Figure 3-2, and Figure 3-3, along with the known concentrations of their components, principal component regression (PCR) models were prepared for measuring U(III), U(IV), and U(VI) in solution. Figure 3-10 shows the results of each of these models in the NaKMg-Cl eutectic solution. The linearity of each of the regressions (measured vs known values) shown in the parity plots of this figure indicate excellent model fit, with each showing a slope of near unity, and y-intercept of near zero for each (slope = 1 and y-intercept = 0 is ideal). The model regression statistics are shown in Table 3-3.

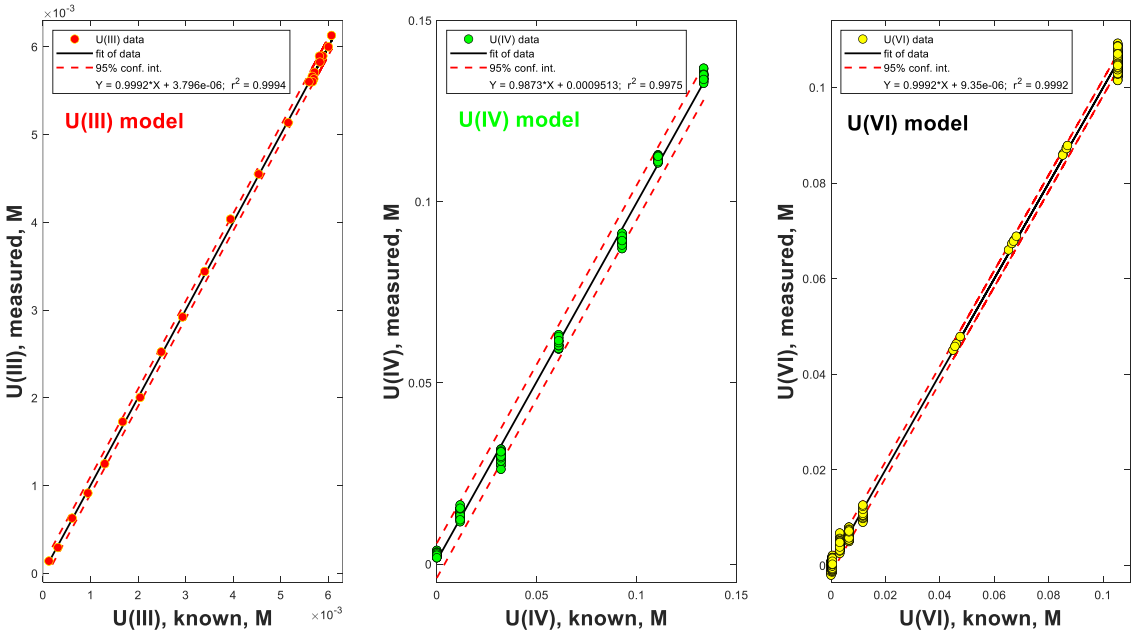

Figure 3-10. Parity plots for the principal component regression modeling of U(III), U(IV), and U(VI) based on UV-vis spectra in NaKMg-Cl eutectic solution.

Using the Raman data shown in Figure 3-3, along with the known solution composition of uranium, a PCR model was prepared for U(VI) in solution. Figure 3-11 shows the results of each of these models in the NaKMg-Cl eutectic solution. The linearity of the regression (slope = 0.999, y-intercept = 3×10^{-5}) indicates excellent model fit. The model regression statistics are shown in Table 3-3.

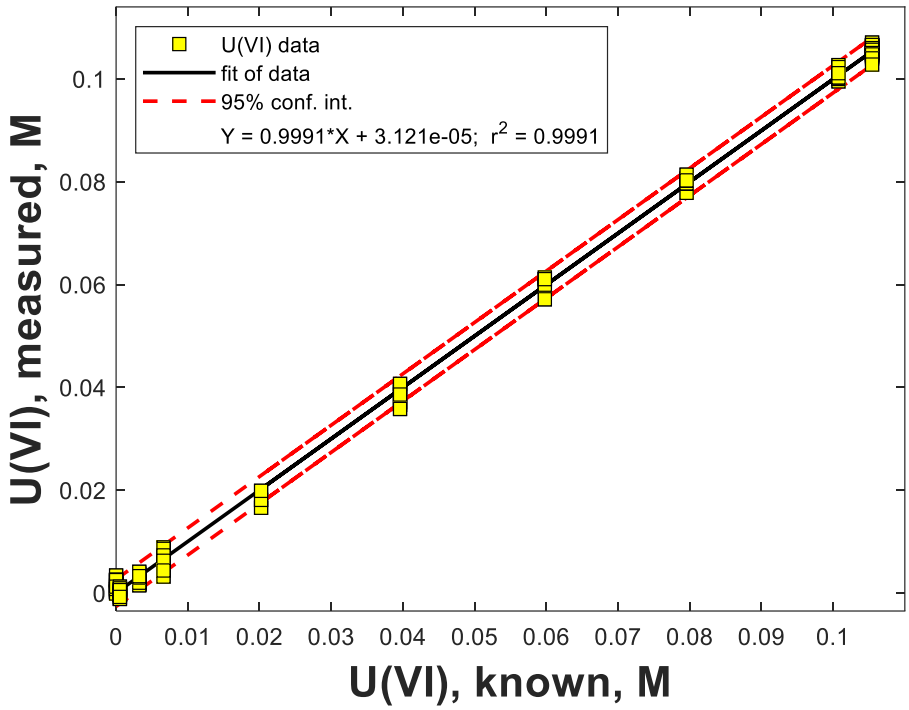

Figure 3-11. Parity plot for the principal component regression (PCR) modeling of U(VI) Raman spectra in NaKMg-Cl eutectic solution.

3.3.2. Advancing models to include interfering species

The effect of adding chemical constituents on the ability to determine the uranium composition was evaluated. The dataset containing variable U(IV) and U(VI) was used for this purpose by synthetically adding UV-vis spectra of lanthanides of known concentration. The resultant spectra described in Figure 3-5 were used to form PCR regression models for U(IV) and U(VI).

The result of adding spectral variation to the U(IV)/U(VI) training sets has no significant effect on the resulting U(IV) and U(VI) model performance. The resulting models had essentially the same metrics of performance as the U(IV) and U(VI) models without lanthanides added and are included in Table 3-3. The reason the addition of more spectral variation does not affect the error statistics (root mean square error of calibration (RMSEC) and root mean square error of cross-validation (RMSECV)) is that while these do add additional intensity at various wavelengths and overlap with the U(IV) and U(VI) spectral bands, they are added in constant contribution for each of the U spectra. In this way they do not add variable “noise” between each spectrum, and therefore they do not change the principal component regression analysis which captures the variation within the spectral dataset. If, on the other hand, the lanthanides were experimentally added to the solutions containing U, then the experimental variation would be expected to be reflected as an increase in uncertainty in the U(IV) and U(VI) concentrations in the training set, and then the RMSEC/CV values would be expected to have an increased error based on the error of the training set standards the models are based on.

Table 3-3. Metrics for model performance of U(III), U(IV), and U(VI).

analyte	spectral method	model description	PCs	RMSEC, RMSECV, r^2
U(III)	UV-vis	PCR: mean-centering	2	0.00005, 0.00005, 0.999
U(IV)	UV-vis	PCR: mean-centering	2	0.00121, 0.00416, 0.998
U(IV) + added lanthanides	UV-vis	PCR: mean-centering	2	0.00122, 0.00417, 0.998
U(VI)	UV-vis	PCR: mean-centering	2	0.00072, 0.00197, 0.999
U(VI) + added lanthanides	UV-vis	PCR: mean-centering	2	0.00082, 0.00221, 0.999
U(VI)	Raman	PCR: 1st derivative, mean-centering	2	0.00130, 0.00137, 0.999

When evaluating the uncertainty of model results, a key metric is the RMSECV. This value can be interpreted as the ±concentration error value of modeling outputs.[28] Results here show uncertainties at or below mM concentrations. Section 4 will discuss this in the context of MC&A as well as recommendations for next steps.

3.3.3. Application of chemometric models on full spectral datasets containing mixtures of U(III), U(IV), and U(VI)

U(IV) additions to NaKMg-Cl eutectic

Applying the regression models developed and described in Section 3.3.1, the solution composition for the full dataset representing the experiments in Figure 3-3 can be directly measured. This is a key demonstration of following a complex chemical system where the dynamic behavior of U can significantly complicate quantification. Here, the incomplete dissolution of U as well as the oxidation of IV to VI are presented. Both behaviors could add notable challenges to accurate MC&A of U. Despite these challenges, the optical monitoring combined with chemometric modeling provides powerful insight into solution composition.

The UV-vis spectra in Figure 3-3 show the U(IV) convert to U(VI) in solution, over a ~24-hour timeframe. By applying the appropriate U(IV) and U(VI) models, the concentration of the U(IV) and U(VI) are determined, with results shown in Figure 3-12A. The black colored dashed line represents the concentration of U(IV) added to the NaKMg-Cl eutectic solution as UCl_4 in six sequential steps. The green curve represents the measured U(IV) concentration using the regression models described above for U(IV). It is immediately apparent that the measured U(IV) concentration (green line) does not equal the analytical amount added (black dashed line). In addition, after the fourth U(IV) addition (labeled U(IV)-4 in Figure **3-12**) the concentration of U(IV) is seen to decrease in value starting at the 4-hour mark to approximately 23-hour time.

The U(VI) concentration of the solution depicted in Figure 3-3 was also directly measured using the regression model described in the section above. The result shown in Figure 3-12 shows that the U(VI) (yellow curve) increases in concentration starting at the approximate time that the U(IV) decreased in concentration. The is a direct (1:1) correlation between the U(IV) disappearance and the U(VI) appearance. The U(VI) growth stops at the ~23-hour mark, corresponding to the time the U(IV) is completely consumed.

The magenta curve in Figure 3-12, is the sum of the concentration of the two U species (U(IV) + U(VI)). The sum of U(IV) and U(VI) (magenta curve) shows mass balance is achieved for most of the period between 7 hours and 23 hours of this experiment. There is a definite period just after the U(IV) fourth

addition (labeled U(IV)-4), from 4 hours to ~7 hours, that the measured total U in solution (magenta curve) does not equal, and is less than, the analytical amount of U added (black dashed line). This discrepancy amounts to ~ 15% of the U in solution at that point in the experiment. This difference can be explained by the observation that some of the U(IV) added precipitated from solution, as shown in the photograph in Figure 3-12B, which was taken just after the U(IV) fourth addition (U(IV)-4) at the 4-hour mark. During the next interval of time for this experiment, the mass balance between the total U measured (magenta curve) and the known amount added (black dashed line) comes into agreement, which is explained by the observation that all the uranium precipitation redissolved into solution, as shown in the photograph (Figure 3-12C) taken just prior to the fifth U(IV) addition at ~23-hour time mark. The observation of the clear-yellow solution shown in Figure 3-12C also indicates the uranyl U(VI) species was formed. The U(VI) formation was confirmed by the band position observed in the Raman spectrum of this solution (Figure 3-3B), at 842 cm^{-1}.

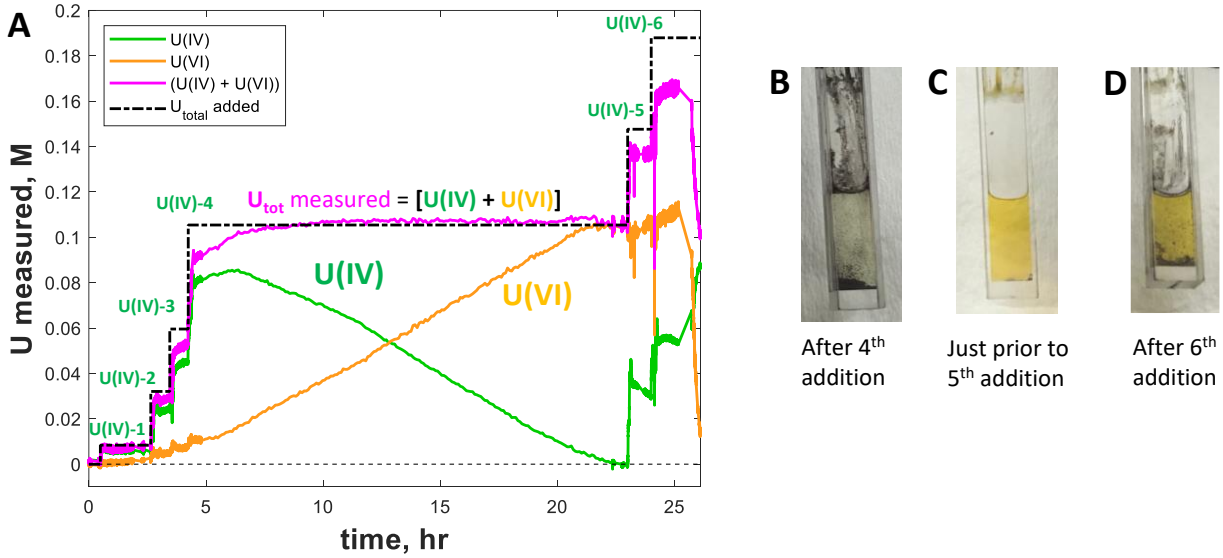

Figure 3-12. The direct measurement of U(IV) and U(VI) in a NaKMg-Cl eutectic. U(IV) was added (as UCl_4 salt) in six sequential steps (U(IV)-1 through U(IV)-6, black dashed line), while U(IV) (green curve), U(VI) (yellow curve), and their sum (magenta curve) were directly and quantitatively measured via chemometric regression models.

U(III) and U(IV) added to NaKMg-Cl eutectic

As another demonstration of a challenging salt system for the accurate quantification of U, models were applied to the sequential addition of U(IV) followed by the sequential addition of U(III) in NaKMg-Cl eutectic melt. This was described in Figure 3-9 and related text. This figure has been replotted in Figure 3-13A to show the progression of added solution components (soln-1 through soln-6) along with labels for the band maxima for the various solution species, U(III), U(IV), and U(VI). Applying the regression models developed and described in Section 3.3.1, the solution composition for the full dataset representing the experiments in Figure 3-13A can be directly measured. The UV-vis spectra in Figure 3-13A show four sequential additions of UCl_4 (labeled soln-1 through soln-4 in Figure 3-13A), followed by two sequential additions of UCl_3 (labeled soln-5 and soln-6). By applying the U(III), U(IV), and U(VI) models, the concentration of all the U species in various oxidation states were determined, with results shown in Figure **3-13**B. The green-dashed line indicates the analytical amount of U(IV) added (as UCl_4 solid), the red-

dashed line indicates the U(III) added (as UCl_3 solid), with the sum of U(III) and U(IV) indicated as the black dashed line.

From Figure 3-13B, it is apparent that the measured U(IV) (green-circle symbols) matches the known additions of U(IV) (green-dashed line) up through the fourth addition of U(IV) (labeled (U(IV)-1 through U(IV)-4 in Figure 3-13B). In addition to U(IV), there is a small amount of U(VI) measured (yellow-square symbols) for the first four additions of U(IV), consistent with the description above showing U(VI) is formed when U(IV) is added to the NaKMg-Cl eutectic melt. In this case, the contact time was several minutes between additions, so the formation of U(VI) from U(IV) was limited.

After the U(IV) additions, U(III) was added in two sequential additions of UCl_3 solid samples, as shown in Figure 3-13B (labeled U(III)-5 and U(III)-6). The analytical amount added is indicated as the red-dashed line in the figure. Interestingly, very little U(III) is measured in solution based on the chemometric analysis (indicated as the red-diamond symbols in figure). However, upon addition of the U(III), the measured U(IV) increases, and the U(VI) present from previous U additions decreased. This indicates immediate conversion of U(III) to U(IV), presumably due to the reaction of U(III) + U(VI) converting to U(IV).

The reaction scheme depicted below summarizes the observations of the initial conversion of U(IV) to U(VI), which is a slow reaction, under our conditions required 24 hours for complete conversion to happen. The second step is the fast conversion of U(III) to U(IV) aided by the reduction of U(VI).

$$U(IV) \rightarrow U(VI) \qquad \text{Slow Reaction}$$
$$U(III) + U(VI) \rightarrow 2U(IV) \qquad \text{Fast Reaction}$$

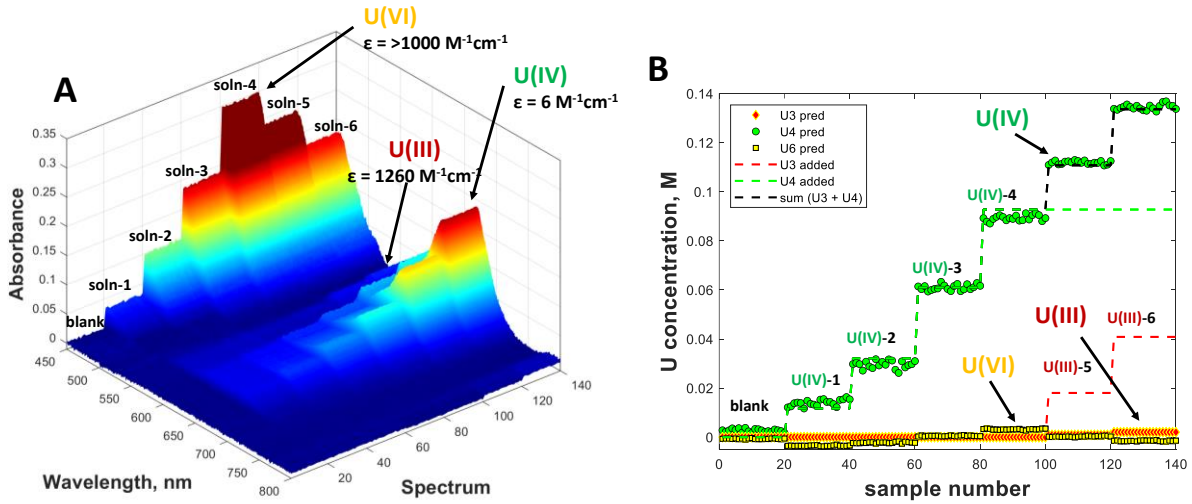

Figure 3-13. Validation set for U(III)/U(IV)/U(VI) in LiK-Cl salt eutectic. Indicates ability to account for U species originally added to matrix, and ability to account for complex chemistry within matrix.

4. UNCERTAINTIES, BENEFITS AND MC&A APPLICATIONS

Recent calculations and demonstrations completed by N. Shoman indicate a high level of difficulty in achieving the 0.1% target accountancy error within liquid fuel MSRs. That result is echoed here, though it is also important to understand the effective value of on-line monitoring techniques. This section covers two topics: 1) How the uncertainty of optically monitoring concentrations compares to traditional MC&A requirements and 2) The role and value of on-line monitoring in the MC&A of an MSR.

As covered in section 3, limits of detection for U fall in the range of mM for U(IV) and U(VI) and sub-mM for U(III). In terms of weight percent that falls roughly around 0.002 – 0.3 wt% U of the total amount of salt in the studies here, though it should be noted that vendors may run anywhere from 5 wt% to significantly higher U wt%, which is notably higher than the concentrations used here to determine LODs and accuracy. In molten salt systems where vendors are proposing these large U loadings of 5% and higher, calculated limits of detection show optical techniques are highly applicable. In fact, these low limits of detection may mean it will be more important to engineer probes and data analysis approaches to compensate for the very high signal anticipated for U without saturating detectors or leaving linear response ranges.

However, it is also important to keep in mind the errors associated with measurement. In this case chemometric models were created to quantify U present in the salt melts. Table 3-3 provides a list of calculated RMSECV values from the quantification models. The RMSECV of a given model can be interpreted as a ± error value on the measurement.[28] Here, these values range from ±0.05 mM (U III) to ±4 mM (U(IV)). These values remained consistent between models of pure U systems and systems where added fission product simulants interfered with U fingerprints. Based on an example system where the highest concentration of U is 0.34 M (5 wt%), a 0.05-4 mM error represents a reasonable relative error of 0.01 to 1.29% for optical characterization and process control means. Note, the highest concentration characterized in this work was 0.1 M, future work can expand to higher concentrations but for the purposes of this section, calculated uncertainties are extrapolated. However, these errors may still fall short of traditional MC&A goals. Comparing this to targeted accountancy goals of 0.1%, it is clear that it may be difficult to pick up very small changes in concentration.

For comparison to the spectroscopic sensors described here, relative errors for measurement of U and Pu in aqueous fuel reprocessing systems have been reported. For UV-vis measurement of Pu(IV) in nitric acid solution, relative errors ranging from 0.67%[23] to 1.5 - 1.7%[29-30] were reported. For measurements of U(VI) in nitric acid, relative errors of 0.82% were reported for Raman[30] and 0.75% for UV-vis.[27] For U(IV) the relative errors were reported ranging from 0.37% to 0.93% for UV-vis.[9, 29] It should be noted, these measurements were performed using spectrometers that were not specifically optimized for the purposes of achieving the lowest detection limits and uncertainties in measurement. To accurately assess the minimum uncertainty possible for optical spectroscopic systems, a spectrometer system optimally designed for this purpose should be used.

Furthermore, errors and uncertainties discussed above account only for concentration measurements. To complete a mass balance, this data must be paired with measurements of volume and density. Errors from all measurements would then need to be propagated out in mass calculations. While it is not the focus of this report to discuss methods of volume and density measurement, it must be noted that these measurements may come with significant error and further challenge the 0.1% MC&A goal.

In light of these uncertainties, it is valuable to discuss the utility of optical spectroscopy-based monitoring as an MC&A tool. While this approach may not meet the traditional 0.1% accountancy goal, it can still provide essential insight into chemical composition and trends within an MSR. Here the benefits are two-fold, first these techniques can, with low limits of detection, provide continuous feedback on salt composition. This can provide immediate insight into abbreviated or possibly protracted diversions. Secondly, these techniques can be used in combination with off-line analysis to provide comprehensive accounting of nuclear material. This is particularly important in MSRs where complex salt chemistry of actinides can impact representativeness of collected salt samples. For example, if actinides are precipitating

and collecting in an area that does not get sampled, analysis of the collected sample will indicate too low a concentration of targets. However, partnering on-line data can reveal corrosion product precursors or other indications that can account for possible location of “missing” materials. Overall, optical spectroscopy as an on-line tool can, at the very least, provide a means for confident and fast tracking of material and composition trends.

5. CONCLUSIONS

Here the application of optical techniques to molten salt systems for the quantification of uranium was demonstrated. Specifically, the combined techniques of UV-vis absorbance and Raman spectroscopy are used. These provide insight into U speciation, oxidation state, and concentration. Limits of detection are determined to be in the mM range for the various U oxidation states within the chloride melts explored here. Furthermore, representative industry salts from TerraPower were characterized and optical spectroscopy was found to provide valuable insight into salt composition. All data was used to build and validate models for the real-time characterization of U within salts. Uncertainties indicate high precision is possible with optical approaches, though values will still have trouble meeting 0.1% accountability targets, particularly after propagating errors from volume and density measurements. However, optical techniques still provide a highly valuable pathway to 1) monitoring for trends indicating short or protracted diversions and 2) identifying chemistry complexities that can indicate precipitated or plated out actinides are impacting material accounting; all in addition to general quantification with uncertainties in the neighborhood of 1% for U species.

This work lays the foundation for using optical techniques as a key component to support on-line or comprehensive MC&A of molten salts. Further improvement of optical techniques as targeted actinide monitoring tools includes optimizing spectrometers for targets of interest, work here utilized standard instruments where sensitivity and resolution could be substantially improved in the optical ranges for U response. Additionally, expanding chemometric models to both explore wider ranges of U concentration and characterize U within systems utilizing advanced oxidation state control could improve uncertainties.

The PNNL team is collaborating with industry partners to apply optical techniques to representative salt systems. That is demonstrated within this report with the characterization of salts provided by TerraPower. Optical techniques show significant promise in this area, and TerraPower has expressed continued interest to explore applications to additional salts or take steps towards integrating optical probes into salt loops. Future work focusing on these areas is recommended by the PNNL team.

6. ACKNOWLEDGEMENTS

This work was funded by the Department of Energy Office of Nuclear Energy's Advanced Reactor Safeguards Campaign. Pacific Northwest National Laboratory (PNNL) is operated by Battelle Memorial Institute for the DOE under contract DE-AC05-76RL01830.

The team would also like to acknowledge and thank TerraPower for providing a variety of salt samples allowing the team to explore applications to representative salt systems.

7. REFERENCES

1. Schroll, C. A.; Lines, A. M.; Heineman, W. R.; Bryan, S. A., Absorption spectroscopy for the quantitative prediction of lanthanide concentrations in the 3 LiCl - 2 CsCl eutectic at 723 K. *Anal Methods-Uk* **2016,** *8* (43), 7731-7738.
2. Schroll, C. A.; Chatterjee, S.; Levitskaia, T. G.; Heineman, W. R.; Bryan, S. A., Electrochemistry of Europium(III) Chloride in 3 LiCl - NaCl, 3 LiCl-2 KCl, LiCl - RbCl, and 3 LiCl-2 CsCl Eutectics at Various Temperatures. *Journal of the Electrochemical Society* **2017,** *164* (8), H5345-H5352.
3. Schroll, C. A.; Chatterjee, S.; Levitskaia, T. G.; Heineman, W. R.; Bryan, S. A., Electrochemistry and Spectroelectrochemistry of Europium(III) Chloride in 3 LiCl - 2 KCl from 643 to 1123 K. *Anal Chem* **2013,** *85* (20), 9924-9931.
4. Schroll, C. A.; Chatterjee, S.; Levitskaia, T.; Heineman, W. R.; Bryan, S. A., Spectroelectrochemistry of $EuCl_3$ in Four Molten Salt Eutectics; 3 LiCl-NaCl, 3 LiCl-2 KCl, LiCl-RbCl, and 3 LiCl-2 CsCl; at 873 K. *Electroanal* **2016,** *28* (9), 2158-2165.
5. Nagai, T.; Uehara, A.; Fujii, T.; Yamana, H., Reduction behavior of UO_2^{2+} in molten LiCl – RbCl and LiCl – KCl eutectics by using tungsten. *Journal of Nuclear Materials* **2013,** *439* (1), 1-6.
6. Polovov, I. B.; Volkovich, V. A.; Charnock, J. M.; Kralj, B.; Lewin, R. G.; Kinoshita, H.; May, I.; Sharrad, C. A., In Situ Spectroscopy and Spectroelectrochemistry of Uranium in High-Temperature Alkali Chloride Molten Salts. *Inorganic Chemistry* **2008,** *47* (17), 7474-7482.
7. Park, Y. J.; Bae, S. E.; Cho, Y. H.; Kim, J. Y.; Song, K., UV–vis absorption spectroscopic study for on-line monitoring of uranium concentration in LiCl–KCl eutectic salt. *Microchemical Journal* **2011,** *99* (2), 170-173.
8. Bryan, S. A.; Levitskaia, T. G.; Johnsen, A. M.; Orton, C. R.; Peterson, J. M., Spectroscopic monitoring of spent nuclear fuel reprocessing streams: an evaluation of spent fuel solutions via Raman, visible, and near-infrared spectroscopy. *Radiochim Acta* **2011,** *99* (9), 563-571.
9. Lines, A. M.; Hall, G. B.; Asmussen, S.; Allred, J.; Sinkov, S.; Heller, F.; Gallagher, N.; Lumetta, G. J.; Bryan, S. A., Sensor Fusion: Comprehensive Real-Time, On-Line Monitoring for Process Control via Visible, Near-Infrared, and Raman Spectroscopy. *ACS Sens* **2020,** *5* (8), 2467-2475.
10. Lines, A. M.; Hall, G. B.; Sinkov, S. I.; Levitskaia, T.; Gallagher, N. B.; Lumetta, G. J.; Bryan, S. A., Overcoming oxidation state dependent spectral interferences: On-line monitoring of U(VI) reduction to U(IV) via Raman and UV-vis spectroscopy *Ind. Eng. Chem. Res.* **2020,** *59*, 8894-8901.
11. Lines, A. M.; Nelson, G. L.; Casella, A. J.; Bello, J. M.; Clark, S. B.; Bryan, S. A., Multivariate Analysis To Quantify Species in the Presence of Direct Interferents: Micro-Raman Analysis of HNO3 in Microfluidic Devices. *Anal Chem* **2018,** *90* (4), 2548-2554.
12. Lines, A. M.; Tse, P.; Felmy, H. M.; Wilson, J. M.; Shafer, J.; Denslow, K. M.; Still, A. N.; King, C.; Bryan, S. A., Online, Real-Time Analysis of Highly Complex Processing Streams: Quantification of Analytes in Hanford Tank Sample. *Ind Eng Chem Res* **2019,** *58* (47), 21194-21200.
13. Tse, P.; Bryan, S. A.; Bessen, N. P.; Lines, A. M.; Shafer, J. C., Review of on-line and near real-time spectroscopic monitoring of processes relevant to nuclear material management. *Anal Chim Acta* **2020,** *1107*, 1-13.
14. Paviet, P.; Hartmann, T.; Lines, A. M.; Bryan, S. A.; Felmy, H. M.; Glezakou, V.-A.; Nguyen, M.-T.; Medina, A.; Branch, S. D. *Corrosion of Molten Salt Containment Alloys - Fundamental Mechanisms for Corrosion Control and Monitoring*; PNNL-30379; Pacific Northwest National Laboratory: Richland, Washington, 2020.
15. Shirai, O.; Iwai, T.; Suzuki, Y.; Sakamura, Y.; Tanaka, H., Electrochemical behavior of actinide ions in LiCl–KCl eutectic melts. *Journal of Alloys and Compounds* **1998,** *271-273*, 685-688.
16. Serp, J.; Konings, R. J. M.; Malmbeck, R.; Rebizant, J.; Scheppler, C.; Glatz, J. P., Electrochemical behaviour of plutonium ion in LiCl–KCl eutectic melts. *Journal of Electroanalytical Chemistry* **2004,** *561*, 143-148.

17. Bourgès, G.; Lambertin, D.; Rochefort, S.; Delpech, S.; Picard, G., Electrochemical studies on plutonium in molten salts. *Journal of Alloys and Compounds* **2007,** *444-445*, 404-409.
18. Polovov, I. B.; Sharrad, C. A.; May, I.; Vasin, B. D.; Volkovich, V. A.; Griffiths, T. R., Spectroelectrochemical Study of Uranium and Neptunium in LiCl-KCl Eutectic Melt. *ECS Transactions* **2007,** *3* (35), 503-511.
19. Lines, A.; Bryan, S.; Felmy, H.; Branch, S. *On-line Monitoring for Molten Salt Reactor MC&A: Optical Spectroscopy-Based Approaches*; Pacific Northwest National Laboratory, Richland, WA (United States): 2021.
20. Nagai, T.; Uehara, A.; Fujii, T.; Shirai, O.; Sato, N.; Yamana, H., Redox Equilibrium of U4+/U3+ in Molten NaCL-2CsCL by UV-Vis Spectrophotometry and Cyclic Voltammetry. *Journal of Nuclear Science and Technology* **2005,** *42* (12), 1025-1031.
21. Harris, D. C., *Quantitative chemical analysis*. 7 ed.; W.H. Freeman and Co.: New York, NY, 2007.
22. Nagai, T.; Fujii, T.; Shirai, O.; Yamana, H., Study on Redox Equilibrium of UO2 2+/U2 + in Molten NaCl-2CsCl by UV-Vis Spectrophotometry. *Journal of Nuclear Science and Technology* **2004,** *41* (6), 690-695.
23. Lines, A. M.; Adami, S. R.; Sinkov, S. I.; Lumetta, G. J.; Bryan, S. A., Multivariate Analysis for Quantification of Plutonium(IV) in Nitric Acid Based on Absorption Spectra. *Anal Chem* **2017,** *89* (17), 9354-9359.
24. Nelson, G. L.; Asmussen, S. E.; Lines, A. M.; Casella, A. J.; Bottenus, D. R.; Clark, S. B.; Bryan, S. A., Micro-Raman Technology to Interrogate Two-Phase Extraction on a Microfluidic Device. *Anal Chem* **2018,** *90* (14), 8345-8353.
25. Schroll, C. A.; Lines, A. M.; Heineman, W. R.; Bryan, S. A., Absorption spectroscopy for the quantitative prediction of lanthanide concentrations in the 3LiCl–2CsCl eutectic at 723 K. *Anal Methods-Uk* **2016,** *8* (43), 7731-7738.
26. Nelson, G. L.; Lackey, H. E.; Bello, J. M.; Felmy, H. M.; Bryan, H. B.; Lamadie, F.; Bryan, S. A.; Lines, A. M., Enabling Microscale Processing: Combined Raman and Absorbance Spectroscopy for Microfluidic On-Line Monitoring. *Anal Chem* **2021,** *93* (3), 1643-1651.
27. Lines, A. M.; Hall, G. B.; Sinkov, S.; Levitskaia, T.; Gallagher, N. B.; Lumetta, G. J.; Bryan, S. A., Overcoming Oxidation State-Dependent Spectral Interferences: Online Monitoring of U(VI) Reduction to U(IV) via Raman and UV-vis Spectroscopy. *Ind Eng Chem Res* **2020,** *59* (19), 8894-8901.
28. Faber, N. M.; Bro, R., Standard error of prediction for multiway PLS 1. Background and a simulation study. *Chemometr Intell Lab* **2002,** *61* (1-2), 133-149.
29. Mattio, E.; Caleyron, A.; Miguirditchian, M.; Lines, A. M.; Bryan, S. A.; Lackey, H. E.; Rodriguez-Ruiz, I.; Lamadie, F., Microfluidic In Situ Spectrophotometric Approaches to Tackle Actinides Analysis in Multiple Oxidation States. *Applied Spectroscopy* **2022**.
30. Cipiti, B. B.; McDaniel, M.; Bryan, S. A.; Pratt, S. H., Cost Effective Implementation of Spectroscopy-Based Process Monitoring. Albuquerque, NM, 2014.